Digital recording and numerical reconstruction of holograms

REVIEW ARTICLE

Digital recording and numerical reconstruction of holograms

Ulf Schnars[1,3] and Werner P O Jüptner[2]

[1] Im Grund 7, D-27628 Hagen, Germany
[2] Bremer Institut für Angewandte Strahltechnik (BIAS), Klagenfurter Straße 2, D-28359 Bremen, Germany

E-mail: schnars@t-online.de

Abstract

This article describes the principles and major applications of digital recording and numerical reconstruction of holograms (digital holography).

Digital holography became feasible since charged coupled devices (CCDs) with suitable numbers and sizes of pixels and computers with sufficient speed became available. The Fresnel or Fourier holograms are recorded directly by the CCD and stored digitally. No film material involving wet-chemical or other processing is necessary. The reconstruction of the wavefield, which is done optically by illumination of a hologram, is performed by numerical methods. The numerical reconstruction process is based on the Fresnel–Kirchhoff integral, which describes the diffraction of the reconstructing wave at the micro-structure of the hologram.

In the numerical reconstruction process not only the intensity, but also the phase distribution of the stored wavefield can be computed from the digital hologram. This offers new possibilities for a variety of applications. Digital holography is applied to measure shape and surface deformation of opaque bodies and refractive index fields within transparent media. Further applications are imaging and microscopy, where it is advantageous to refocus the area under investigation by numerical methods.

Keywords: digital holography, holographic interferometry

1. Introduction

Dennis Gabor [1–3] invented holography in 1948 as a method for recording and reconstructing the amplitude and phase of a wavefield. The word *holography* is derived from the Greek words 'holos' meaning 'whole' or 'entire' and 'graphein' meaning 'to write'.

A hologram is the photographically or otherwise recorded interference pattern between a wavefield scattered from the object and a coherent background, called the reference wave. A hologram is usually recorded on a flat surface, but contains information about the entire three-dimensional wavefield.

[3] U Schnars works for AIRBUS Deutschland GmbH, but contributed to this work as a private individual.

This information is coded in the form of bright and dark microinterferences, usually not visible for the human eye due to the high spatial frequencies. The object wave can be reconstructed by illuminating the hologram with the reference wave again. This reconstructed wave is indistinguishable from the original object wave. An observer sees a three-dimensional image which exhibits all the effects of perspective and depth of focus.

In the original set-up of Gabor the reference wave and object wave are located along the axis normal to the photographic plate. This leads to a reconstructed image superimposed by the bright reconstruction wave and a second image, the so-called 'twin image'. Significant improvements of this in-line holography were made by Leith

and Upatnieks [4, 5], who introduced an off-axis reference wave. With their set-up the two images and the reconstruction wave are spatially separated.

One major application of holography is holographic interferometry (HI), developed in the late 1960s by Stetson and Powell [6, 7] and others. With HI it became possible to map the displacements of rough surfaces with an accuracy of a fraction of a micrometre. It is also possible to make interferometric comparisons of stored wavefronts that exist at different times.

The development of computer technology made it possible to transfer either the recording process or the reconstruction process into the computer. The first approach led to computer generated holography (CGH), which allows us to generate artificial holograms by numerical methods. These computer generated holograms are then optically reconstructed. This technique is not considered here: we refer the interested reader to the literature, see, for example, [8–10].

Numerical hologram reconstruction was initiated by Yaroslavskii *et al* [11–13] at the early 1970s. They sampled optically enlarged parts of in-line and Fourier holograms recorded on a photographic plate. These digitized 'conventional' holograms were reconstructed numerically. Onural and Scott [14–16] improved the reconstruction algorithm and applied this method to particle measurement. Haddad *et al* [73] described a holographic microscope based on numerical reconstruction of Fourier holograms.

A big step forward was the development of direct recording of Fresnel holograms with charged coupled devices (CCDs) by Schnars and Jüptner [17, 18]. This method now enables full digital recording and processing of holograms, without any photographic recording as an intermediate step. Within the scope of this article digital sampling and numerical hologram reconstruction is called *digital holography*.

Schnars and Jüptner applied their method to interferometry and demonstrated that digital hologram reconstruction offers much more possibilities than conventional (optical) processing. The phases of the stored light waves can be calculated directly from the digital holograms, without generating phase-shifted interferograms [19, 20]. Other methods of optical metrology, such as shearography or speckle photography, can be derived numerically from digital holograms [21]. This means that one can choose the interferometric technique (hologram interferometry, shearography or other technique) after hologram recording by mathematical methods.

The use of electronics devices, such as CCDs, for the recording of interferograms was already established in electronic speckle pattern interferometry (ESPI, also called *TV holography*), discovered independently from each other by Butters and Leendertz [22], Macovski *et al* [23] and Schwomma [24]. In this method two speckle interferograms are recorded at different states of the object under investigation. The speckle patterns are subtracted electronically. The resulting fringe pattern has some similarities to that of conventional or digital HI, but the main differences are the speckle appearance of the fringes and the loss of phase in the correlation process. The interference phase has to be recovered with phase-shifting methods [26–28], requiring additional experimental effort (phase-shifting unit). Digital HI and ESPI are competing methods: the image subtraction in ESPI is simpler than the numerical reconstruction of digital
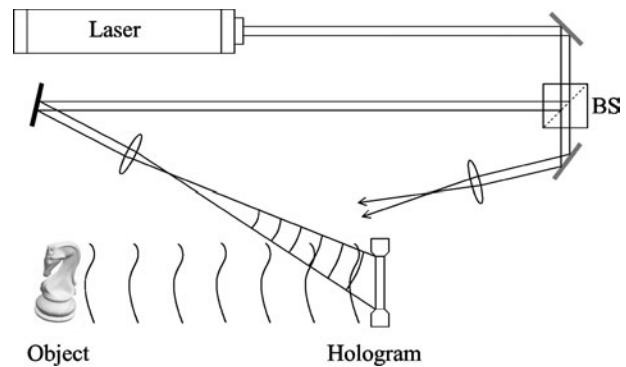

Figure 1. Hologram recording.

holography, but the information content of digital holograms is higher. ESPI is not considered here: we refer to corresponding articles [25, 29, 30].

Since the mid-1990s digital holography has been modified, improved and applied to several measurement tasks [31–97].

Important steps are:

- improvements in the experimental techniques and reconstruction algorithm [31–50],
- applications in deformation analysis and shape measurement [51–55, 71, 111],
- the development of phase-shifting digital holography [56–64],
- applications in imaging, particle tracking and microscopy [65–70, 73, 104],
- measurement of refractive index distributions within transparent media [72, 74, 75],
- applications in encrypting information [76, 77],
- the development of digital light-in-flight holography [78–83],
- the development of comparative digital holography [84].

Recently it has been demonstrated how to reconstruct digital holograms optically using a liquid crystal device (LCD) [84] or a digital micromirror device (DMD) [98].

2. Foundations of holography

2.1. Hologram recording and reconstruction

The general set-up for recording off-axis holograms is shown in figure 1 [99, 100]. Light with sufficient coherence length is split into two partial waves by a beamsplitter (BS). One wave illuminates the object, is scattered and reflected to the recording medium, e.g. a photographic plate. The second wave, called the reference wave, illuminates the plate directly. Both waves are interfering. The interference pattern is recorded, e.g. by chemical development of the photographic plate. The recorded interference pattern is called a hologram.

The original object wave is reconstructed by illuminating the hologram with the reference wave, figure 2. An observer sees a virtual image, which is indistinguishable from the image of the original object. The reconstructed image exhibits all the effects of perspective and depth of focus.
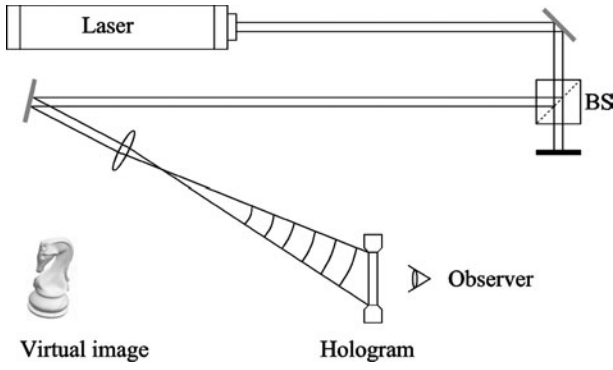
Figure 2. Hologram reconstruction.

The holographic process is described mathematically as follows:

$$O(x, y) = o(x, y) \exp(i\varphi_O(x, y)) \tag{2.1}$$

is the complex amplitude of the object wave with real amplitude o and phase φ_O and

$$R(x, y) = r(x, y) \exp(i\varphi_R(x, y)) \tag{2.2}$$

is the complex amplitude of the reference wave with real amplitude r and phase φ_R.

Both waves interfere at the surface of the recording medium. The intensity is calculated by

$$\begin{aligned}
I(x, y) &= |O(x, y) + R(x, y)|^2 \\
&= (O(x, y) + R(x, y))(O(x, y) + R(x, y))^* \\
&= R(x, y)R^*(x, y) + O(x, y)O^*(x, y) \\
&\quad + O(x, y)R^*(x, y) + R(x, y)O^*(x, y)
\end{aligned} \tag{2.3}$$

where * denotes the conjugate complex. The amplitude transmission $h(x, y)$ of the developed photographic plate (or any other recording media) is proportional to $I(x, y)$:

$$h(x, y) = h_0 + \beta\tau I(x, y) \tag{2.4}$$

where β is a constant, τ is the exposure time and h_0 is the amplitude transmission of the unexposed plate. $h(x, y)$ is also called the hologram function. In digital holography using CCDs as recording medium h_0 can be neglected.

For hologram reconstruction the amplitude transmission has to be multiplied with the complex amplitude of the reconstruction (reference) wave:

$$\begin{aligned}
R(x, y)h(x, y) &= [h_0 + \beta\tau(r^2 + o^2)]R(x, y) \\
&\quad + \beta\tau r^2 O(x, y) + \beta\tau R^2(x, y)O^*(x, y).
\end{aligned} \tag{2.5}$$

The first term on the right side of this equation is the reference wave, multiplied by a factor. It represents the undiffracted wave passing through the hologram (zero diffraction order). The second term is the reconstructed object wave, forming the virtual image. The factor $\beta\tau r^2$ only influences the brightness of the image. The third term produces a distorted real image of the object. For off-axis holography the virtual image, the real image and the undiffracted wave are spatially separated.

2.2. Holographic interferometry

HI is an optical method to observe deformations of opaque bodies or refractive index variations in transparent media, e.g. fluids or gases. HI is a non-contact, non-destructive method with very high sensitivity. Optical path changes up to one hundredth of a wavelength are resolvable.

Two coherent wavefields, which are reflected from two different states of the object, are interfering. This is achieved, for example, in double-exposure holography by the recording of two wavefields on a single photographic plate. The first exposure represents the object in its initial state and the second exposure represents the object in its loaded (e.g. deformed) state. The hologram is reconstructed by illumination with the reference wave. As a result of the superposition of the two holographic recordings with *slightly* different object waves only one image superimposed by interference fringes is reconstructed. From this holographic interferogram the observer can determine optical path changes due to the object deformation or other effects.

In the real time technique the hologram is replaced, after processing, in exactly the same position in which it was recorded. When it is illuminated with the reference wave, the reconstructed virtual image coincides with the object. Interference patterns due to phase changes between the holographically reconstructed initial object wave and the actual object wave are observable in real time.

The following mathematical description is valid for the double exposure and real time techniques. The complex amplitude of the object wave in the initial state is

$$O_1(x, y) = o(x, y) \exp[i\varphi(x, y)] \tag{2.6}$$

where $o(x, y)$ is the real amplitude and $\varphi(x, y)$ is the phase of the object wave.

Optical path changes due to deformations of the object surface can be described by a variation of the phase from φ to $\varphi + \Delta\varphi$. $\Delta\varphi$ is the difference between the initial and actual phase, and is called the *interference phase*. The complex amplitude of the actual object wave is therefore denoted by

$$O_2(x, y) = o(x, y) \exp[i(\varphi(x, y) + \Delta\varphi(x, y))]. \tag{2.7}$$

The intensity of a holographic interference pattern is described by the square of the sum of the complex amplitudes. It is calculated as follows:

$$\begin{aligned}
I(x, y) &= |O_1 + O_2|^2 = (O_1 + O_2)(O_1 + O_2)^* \\
&= 2o^2(1 + \cos(\Delta\varphi)).
\end{aligned} \tag{2.8}$$

Equation (2.8) describes the relation between the intensity of the interference pattern and the interference phase, which contains the information about the deformation.

It is not possible to calculate the interference phase distribution correctly from one single fringe pattern, because the cosine is an even function ($\cos 30° = \cos -30°$) and the sign of the argument is not determined unequivocally. In most practical cases distortions have to be considered in addition. The interference pattern is superimposed by speckle noise and the brightness of the pattern varies due to the profile of the illuminating laser beam. Therefore several techniques have been developed to determine the interference phase by
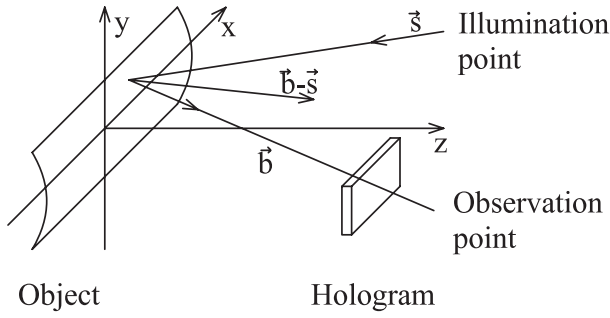
Figure 3. Definition of the sensitivity vector.

Figure 4. Digital holography: (a) recording, (b) reconstruction.

recording additional information. The most commonly used techniques are the various phase-shifting methods [100–102]. Three or more interferograms are reconstructed with mutual phase shifts. The interference phase is calculated from these phase-shifted intensity distributions.

The interference phase is the key to calculate quantities representing the object under investigation. These are the displacement vector field of the surface in the case of opaque bodies or refractive index changes within transparent media. A third application of HI is to measure the shape of bodies (contouring). In the following we describe the application of HI to measure surface displacements. For a detailed description of the other applications we refer to the literature, see, for example, [100].

The relation between the measured interference phase and the displacement vector field $\vec{d}(x, y, z)$ of the object surface under investigation is given by the following equation [100, p 72], [103]:

$$\Delta\varphi(x, y) = \frac{2\pi}{\lambda}\vec{d}(x, y, z)(\vec{b} - \vec{s}) = \frac{2\pi}{\lambda}\vec{d}(x, y, z)\vec{S} \quad (2.9)$$

where $\vec{b}$ and $\vec{s}$ are unit vectors in the illumination and observation directions, see figure 3. The vector $\vec{S}$ is called the *sensitivity vector*. The sensitivity vector is defined only by the geometry of the holographic arrangement. It gives the direction in which the set-up has maximum sensitivity. At each point we measure the projection of the displacement vector onto the sensitivity vector. Equation (2.9) is the basis of all quantitative measurements of the deformation of opaque bodies.

In the general case of a three-dimensional deformation field equation (2.9) contains the three components of $\vec{d}$ as unknown parameters. In this case three interferograms of the same surface with linear independent sensitivity vectors are necessary to determine the displacement. In many practical cases it is not the three-dimensional displacement field, but the deformation perpendicular to the surface, which is of interest. In this case an optimized set-up with parallel illumination and observation direction is used ($\vec{S} = (0, 0, 2)$). The component d_z is then calculated from the interference phase by

$$d_z = \Delta\varphi\frac{\lambda}{4\pi}. \quad (2.10)$$

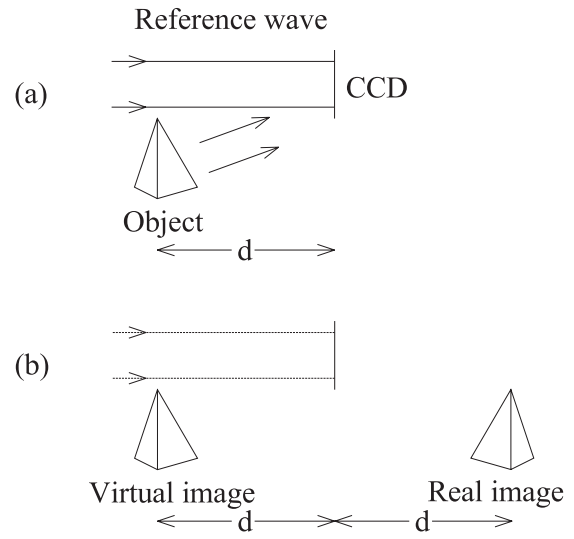A phase variation of 2π corresponds to a deformation of $\lambda/2$.

3. Digital holography

3.1. General principles

A general set-up for digital recording of off-axis holograms is shown in figure 4 [18]. A plane reference wave and the wave reflected from the object are interfering at the surface of a CCD. The resulting hologram is electronically recorded and stored. The object is, in general, a three-dimensional body with diffusely reflecting surface, located at a distance d from the CCD.

In optical reconstruction the virtual image appears at the position of the original object and the real image is formed also at a distance d, but in the opposite direction from the CCD, see figure 4(b).

The diffraction of a light wave at an aperture (in this case a hologram) which is fastened perpendicular to the incoming beam is described by the Fresnel–Kirchhoff integral [105, p 266]:

$$\Gamma(\xi, \eta) = \frac{i}{\lambda}\int_{-\infty}^{\infty}\int_{-\infty}^{\infty} h(x, y)R(x, y)\frac{\exp(-i\frac{2\pi}{\lambda}\rho)}{\rho}$$
$$\times \left(\tfrac{1}{2} + \tfrac{1}{2}\cos\theta\right)\mathrm{d}x\,\mathrm{d}y \quad (3.1)$$

with

$$\rho = \sqrt{(x - \xi)^2 + (y - \eta)^2 + d^2} \quad (3.2)$$

where $h(x, y)$ is again the hologram function and ρ is the distance between a point in the hologram plane and a point in the reconstruction plane, see figure 5. The angle θ is also defined in figure 5. For a plane reference wave $R(x, y)$ is simply given by the real amplitude:

$$R = r + i0 = r. \quad (3.3)$$

The diffraction pattern is calculated at a distance d behind the CCD plane, which means it reconstructs the complex amplitude in the plane of the real image.

Equation (3.1) is the basis for numerical hologram reconstruction. Because the reconstructed wavefield $\Gamma(\xi, \eta)$ is a complex function, both the intensity as well as the phase can be calculated [19]. This is in contrast to the case of optical
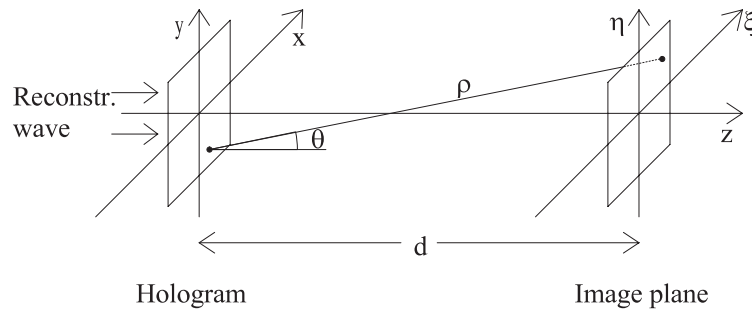
Figure 5. Coordinate system.

hologram reconstruction, in which only the intensity is made visible. This interesting property of digital holography is used in digital HI, see section 4.

There are a few slightly different formulae of the Fresnel–Kirchhoff integral in the literature, which differ, for example, by the sign of the argument of the exponential function ($\exp(+i\ldots)$ instead of $\exp(-i\ldots)$). However, with the '+' sign as well the same expressions result for the intensity and magnitude of the interference phase used in digital HI.

The set-up of figure 4 is often used in digital holography, because a plane wave propagating perpendicularly to the surface of the CCD can be easily arranged in the laboratory. Another advantage is that for this geometry the reconstructed real image has no geometrical distortions (this can be derived from the holographic imaging equations, see, for example, [100, pp 45–8]). Other recording geometries are discussed in section 3.6.

3.2. Reconstruction by the Fresnel transformation

3.2.1. Fresnel approximation. For x and y values as well as for ξ and η values which are small compared to the distance d between the reconstruction plane and the CCD expression (3.2) can be replaced by the first terms of the Taylor series:

$$\rho = d + \frac{(\xi - x)^2}{2d} + \frac{(\eta - x)^2}{2d} - \frac{1}{8}\frac{[(\xi - x)^2 + (\eta - x)^2]}{d^3} + \cdots$$

$$\approx d + \frac{(\xi - x)^2}{2d} + \frac{(\eta - y)^2}{2d} \qquad (3.4)$$

with the additional approximation $\cos\theta \approx 1$, and by replacing the dominator in (3.1) by d the following expression results:

$$\Gamma(\xi, \eta) = \frac{i}{\lambda d}\exp\left(-i\frac{2\pi}{\lambda}d\right)\int_{-\infty}^{\infty}\int_{-\infty}^{\infty} R(x, y)h(x, y)$$
$$\times \exp\left[-i\frac{\pi}{\lambda d}((\xi - x)^2 + (\eta - y)^2)\right]dx\,dy. \qquad (3.5)$$

If we carry out the multiplications in the argument of the exponential under the integral we get

$$\Gamma(\xi, \eta) = \frac{i}{\lambda d}\exp\left(-i\frac{2\pi}{\lambda}d\right)\exp\left[-i\frac{\pi}{\lambda d}(\xi^2 + \eta^2)\right]$$
$$\times \int_{-\infty}^{\infty}\int_{-\infty}^{\infty} R(x, y)h(x, y)\exp\left[-i\frac{\pi}{\lambda d}(x^2 + y^2)\right]$$
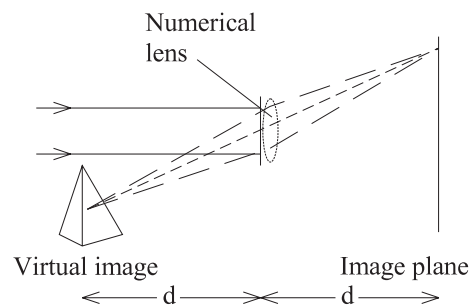$$\times \exp\left[i\frac{2\pi}{\lambda d}(x\xi + y\eta)\right]dx\,dy. \qquad (3.6)$$

Figure 6. Reconstruction of the virtual image.

This equation is called the *Fresnel approximation* or *Fresnel transformation*. It enables reconstruction of the wavefield in a plane behind the hologram, in this case in the plane of the real image. The intensity is calculated by squaring

$$I(\xi, \eta) = |\Gamma(\xi, \eta)|^2. \qquad (3.7)$$

The phase is calculated by

$$\varphi(\xi, \eta) = \arctan\frac{\text{Im}[\Gamma(\xi, \eta)]}{\text{Re}[\Gamma(\xi, \eta)]} \qquad (3.8)$$

where Re denotes the real part and Im the imaginary part.

Reconstruction of the virtual image is also possible by introducing the imaging properties of a lens into the numerical reconstruction process [20, pp 35–6]. This lens corresponds to the eye lens of an observer watching through an optically reconstructed hologram. In the simplest case this lens is located directly behind the hologram, figure 6. The imaging properties of a lens with focal distance f are considered by a complex factor [99, p 259]

$$L(x, y) = \exp\left[i\frac{\pi}{\lambda f}(x^2 + y^2)\right]. \qquad (3.9)$$

For a magnification of 1 a focal distance of $f = d/2$ has to be used. The complex amplitude in the image plane is then calculated by

$$\Gamma(\xi, \eta) = \frac{i}{\lambda d}\exp\left(-i\frac{2\pi}{\lambda}d\right)\exp[-i\frac{\pi}{\lambda d}(\xi^2 + \eta^2)]$$
$$\times \int_{-\infty}^{\infty}\int_{-\infty}^{\infty} R(x, y)L(x, y)h(x, y)\exp\left[-i\frac{\pi}{\lambda d}(x^2 + y^2)\right]$$
$$\times \exp\left[i\frac{2\pi}{\lambda d}(x\xi + y\eta)\right]dx\,dy$$

$$= \frac{i}{\lambda d} \exp\left(-i\frac{2\pi}{\lambda}d\right) \exp\left[-i\frac{\pi}{\lambda d}(\xi^2 + \eta^2)\right]$$

$$\times \int_{-\infty}^{\infty} \int_{-\infty}^{\infty} R(x, y)h(x, y) \exp\left[+i\frac{\pi}{\lambda d}(x^2 + y^2)\right]$$

$$\times \exp\left[i\frac{2\pi}{\lambda d}(x\xi + y\eta)\right] dx \, dy. \tag{3.10}$$

Compared with (3.6) only the sign of the argument of the first exponential function in the integral changes.

3.2.2. Discrete Fresnel transformation. For digitization of the Fresnel transform (3.6) we introduce the following substitutions [13]:

$$\nu = \frac{\xi}{\lambda d}; \qquad \mu = \frac{\eta}{\lambda d}. \tag{3.11}$$

Herewith (3.6) becomes

$$\Gamma(\nu, \mu) = \frac{i}{\lambda d} \exp[-i\pi\lambda d(\nu^2 + \mu^2)]$$

$$\times \int_{-\infty}^{\infty} \int_{-\infty}^{\infty} R(x, y)h(x, y) \exp\left[-i\frac{\pi}{\lambda d}(x^2 + y^2)\right]$$

$$\times \exp[i2\pi(x\nu + y\mu)] dx \, dy. \tag{3.12}$$

The factor $\exp(-i2\pi/\lambda d)$ is omitted, since it only affects the overall phase. It has no effect on the intensity and interference phase of digital HI.

A comparison of (3.12) with the definition of the two-dimensional Fourier transform shows that the Fresnel approximation is, up to a spherical phase factor, the inverse Fourier transformation of $R(x, y)h(x, y) \exp[-i\pi/\lambda d(x^2 + y^2)]$:

$$\Gamma(\nu, \mu) = \frac{i}{\lambda d} \exp[-i\pi\lambda d(\nu^2 + \mu^2)]$$

$$\times \Im^{-1}\left\{R(x, y)h(x, y) \exp\left[-i\frac{\pi}{\lambda d}(x^2 + y^2)\right]\right\}. \tag{3.13}$$

The function Γ can be digitized if the hologram function $h(x, y)$ is sampled on a rectangular raster of $N \times N$ points, with steps Δx and Δy along the coordinates. Δx and Δy are the distances between neighbouring pixels on the CCD in the horizontal and vertical directions. With these discrete values the integrals of (3.12) are converted to finite sums:

$$\Gamma(m, n) = \frac{i}{\lambda d} \exp[-i\pi\lambda d(m^2\Delta\nu^2 + n^2\Delta\mu^2)]$$

$$\times \sum_{k=0}^{N-1} \sum_{l=0}^{N-1} R(k, l)h(k, l) \exp\left[-i\frac{\pi}{\lambda d}(k^2\Delta x^2 + l^2\Delta y^2)\right]$$

$$\times \exp[i2\pi(k\Delta x m\Delta\nu + l\Delta y n\Delta\mu)] \tag{3.14}$$

for $m = 0, 1, \ldots, N-1$; $n = 0, 1, \ldots, N-1$.

According to the theory of Fourier transform among Δx, Δy and $\Delta\nu$, $\Delta\mu$ the following relation exists [106]:

$$\Delta\nu = \frac{1}{N\Delta x}; \qquad \Delta\mu = \frac{1}{N\Delta y}. \tag{3.15}$$

After re-substitution:

$$\Delta\xi = \frac{\lambda d}{N\Delta x}; \qquad \Delta\eta = \frac{\lambda d}{N\Delta y}. \tag{3.16}$$

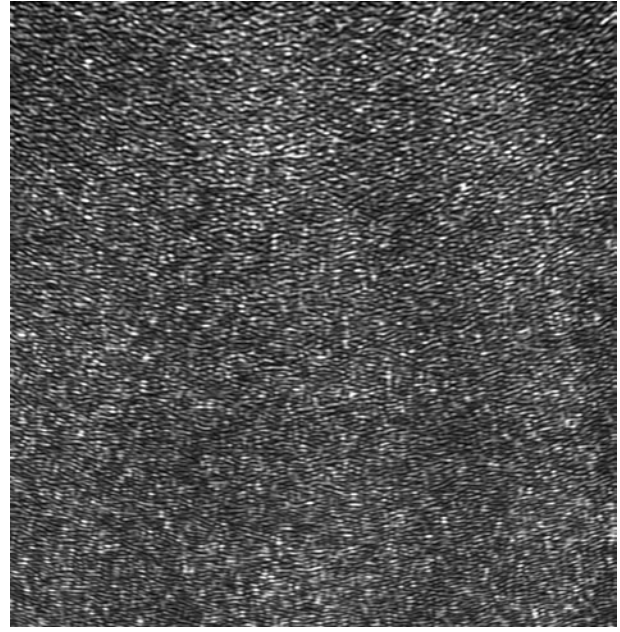**Figure 7.** Digital hologram.

With the use of these equations (3.14) converts to

$$\Gamma(m, n) = \frac{i}{\lambda d} \exp\left[-i\pi\lambda d\left(\frac{m^2}{N^2\Delta x^2} + \frac{n^2}{N^2\Delta y^2}\right)\right]$$

$$\times \sum_{k=0}^{N-1} \sum_{l=0}^{N-1} R(k, l)h(k, l) \exp\left[-i\frac{\pi}{\lambda d}(k^2\Delta x^2 + l^2\Delta y^2)\right]$$

$$\times \exp\left[i2\pi\left(\frac{km}{N} + \frac{ln}{N}\right)\right]. \tag{3.17}$$

This is the discrete Fresnel transform. The matrix Γ is calculated by multiplying $R(k, l)$ with $h(k, l)$ and $\exp[-i\pi/(\lambda d)(k^2\Delta x^2 + l^2\Delta y^2)]$ and applying an inverse discrete Fourier transform to the product. The calculation is done most effectively using the fast Fourier transform (FFT) algorithm. The factor in front of the sum is only affecting the phase and can be neglected for most applications.

A typical digital hologram is shown in figure 7. The hologram is recorded with the geometry of figure 4. The object is placed $d = 1.054$ m from the CCD array of 1024×1024 pixels with pixel size $\Delta x = \Delta y = 6.8$ μm. The wavelength is 632.8 nm. The numerical reconstruction, according to (3.6) resp. (3.17), is demonstrated in figure 8. A real image of the cube used as the object is noticeable. The bright square in the centre is the undiffracted reconstruction wave (zero order) and corresponds to the first term of the right side of (2.5). Because of the off-axis geometry the image is spatially separated from the zero-order term. The virtual image is out of focus in this reconstruction.

An interesting property of holography is that every part of a hologram contains the information about the entire object. This is demonstrated in figures 9 and 10, where only 512×512 pixels and 256×256 pixels are used for reconstruction. The reduction of the pixel number leads to a reduction of the resolution of the reconstructed image. This corresponds to an increase in speckle size due to aperture reduction in optical hologram reconstruction.
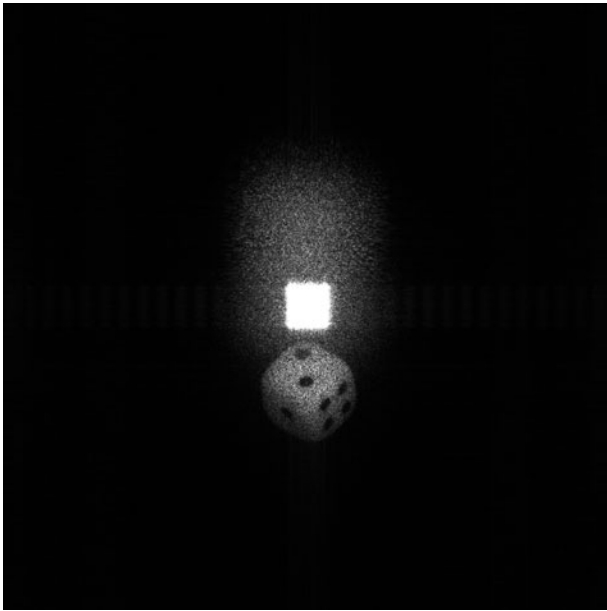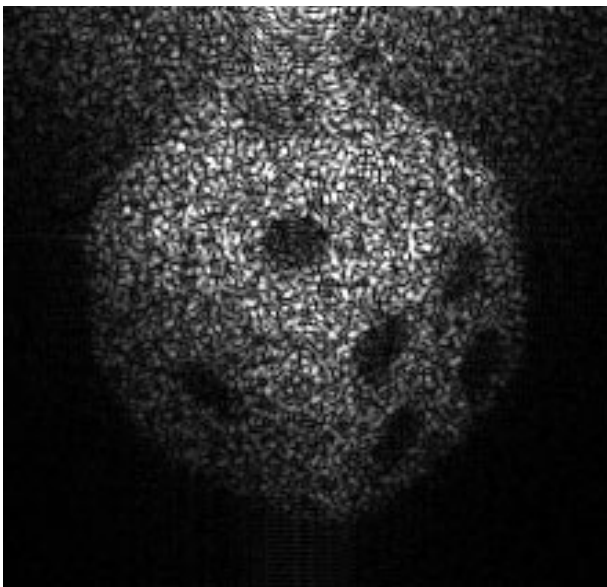
Figure 8. Numerical intensity reconstruction.

Figure 10. Reconstruction with only 256×256 pixels.

Figure 9. Reconstruction with only 512×512 pixels.

According to (3.16) the pixel distances in the reconstructed image, $\Delta\xi$ and $\Delta\eta$, are different from those of the hologram matrix. At first sight it seems to lose (or gain) resolution by applying the numerical Fresnel transform. On closer examination one recognizes that (3.16) corresponds to the diffraction limited resolution of optical systems: the hologram is the aperture of the optical system with side length $N\Delta x$. According to the theory of diffraction at a distance d behind the hologram a diffraction pattern develops. $\Delta\xi = \lambda d / N \Delta x$ is therefore the diameter of the Airy disk (or speckle diameter) in the plane of the reconstructed image, which limits the resolution. This can be regarded as the 'automatic scaling' algorithm, setting the resolution of the image reconstructed by a discrete Fresnel transform always to the physical limit.
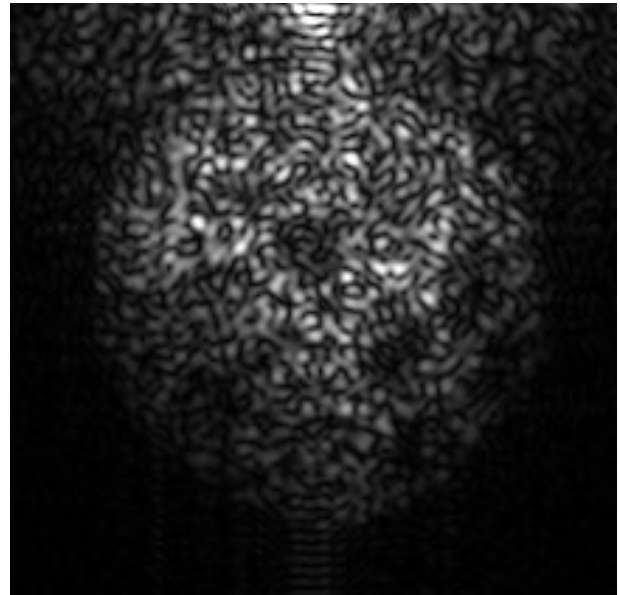
3.3. Reconstruction by the convolution approach

The direct numerical processing of the Fresnel–Kirchhoff integral (3.1) is time consuming. For numerical processing an equivalent formulation is much more suitable. This formulation makes use of the convolution theorem and is called the 'convolution approach' within the scope of this article. The mathematics is well known since the early days of holography. To our knowledge Demetrakopoulos and Mittra [107] first applied this way of processing for numerical reconstruction of suboptical holograms. Later this approach was applied to optical holography [43]. Following this work the diffraction formula (3.1) is a superposition integral:

$$\Gamma(\xi, \eta) = \int_{-\infty}^{\infty} \int_{-\infty}^{\infty} h(x, y) R(x, y) g(\xi, \eta, x, y) \, dx \, dy \tag{3.18}$$

where the impulse response $g(x, y, \xi, \eta)$ is given by

$$g(\xi, \eta, x, y) = \frac{i}{\lambda} \frac{\exp\left[-i\frac{2\pi}{\lambda}\sqrt{d^2 + (x - \xi)^2 + (y - \eta)^2}\right]}{\sqrt{d^2 + (x - \xi)^2 + (y - \eta)^2}} \tag{3.19}$$

where again the approximation $\cos\theta \approx 1$ is used.

Equation (3.19) shows that the linear system characterized by $g(\xi, \eta, x, y) = g(\xi - x, \eta - y)$ is space-invariant: the superposition integral is a convolution. This allows the application of the convolution theorem, which states that the Fourier transform of the convolution of $h \cdot R$ with g is the product of the individual transforms $\Im\{hR\}$ and $\Im\{g\}$. So $\Gamma(\xi, \eta)$ can be calculated by first Fourier transforming $h \cdot R$, then multiplying with the Fourier transform of g, and taking an inverse Fourier transform of this product. The whole process requires all three Fourier transforms, which are effectively carried out using the FFT algorithm.

The numerical realization of the impulse response function is

$$g(k, l) = \frac{i}{\lambda} \frac{\exp\left[-i\frac{2\pi}{\lambda}\sqrt{d^2 + \left(k - \frac{N}{2}\right)^2 \Delta x^2 + \left(l - \frac{N}{2}\right)^2 \Delta y^2}\right]}{\sqrt{d^2 + \left(k - \frac{N}{2}\right)^2 \Delta x^2 + \left(l - \frac{N}{2}\right)^2 \Delta y^2}}.$$
(3.20)

The shift of the coordinates by $N/2$ is on symmetry reasons.

In short notation the reconstruction into the real image plane is

$$\Gamma(\xi, \eta) = \Im^{-1}\{\Im(h \cdot R) \cdot \Im(g)\}.$$
(3.21)

The Fourier transform of $g(k, l)$ can be calculated and expressed analytically:

$$G(n, m)$$
$$= \exp\left\{-i\frac{2\pi d}{\lambda}\sqrt{1 - \frac{\lambda^2\left(n + \frac{N^2\Delta x^2}{2d\lambda}\right)^2}{N^2\Delta x^2} - \frac{\lambda^2\left(m + \frac{N^2\Delta y^2}{2d\lambda}\right)^2}{N^2\Delta y^2}}\right\}.$$
(3.22)

This saves one Fourier transform for reconstruction:

$$\Gamma(\xi, \eta) = \Im^{-1}\{\Im(h \cdot R) \cdot G\}.$$
(3.23)

For the reconstruction of the virtual image a lens transmission factor according to (3.9) has to be considered:

$$\Gamma(\xi, \eta) = \Im^{-1}\{\Im(h \cdot R \cdot L) \cdot G\}.$$
(3.24)

The convolution approach can be applied also to the Fresnel approximation [43].

The pixel sizes of the images reconstructed by the convolution approach are equal to that of the hologram:

$$\Delta\xi = \Delta x; \qquad \Delta\eta = \Delta y.$$
(3.25)

The pixel sizes of the reconstruction are therefore different from those of the Fresnel approximation (3.16). Reconstruction of holograms by the convolution approach result indeed in images with more or less pixels per unit length than those reconstructed by the Fresnel transform. However, the image resolution does not change due to the physical limits discussed at the end of section 3.2.2. The convolution approach is advantageously applied to reconstruct in-line holograms from particle distributions within transparent media. In this case the scale of the reconstructions should be the same for all reconstruction distances in order to localize particles or bubbles within the object volume.

3.4. Suppression of the DC term

The bright square in the centre of figure 8 is the undiffracted reconstruction wave. This zero-order or DC term disturbs the image, because it covers all object parts lying behind. Methods have been developed therefore to suppress this term [44].

To understand the cause of this DC term we consider the hologram formation according to (2.3). The equation is rewritten by inserting the definitions of R and O and multiplying the terms:

$$I(x, y) = r(x, y)^2 + o(x, y)^2 + 2r(x, y)o(x, y)\cos(\varphi_O - \varphi_R).$$
(3.26)

The first two terms lead to the DC term in the reconstruction process. The third term is statistically varying

between $\pm 2ro$ from pixel to pixel in the CCD. The average intensity of all pixels of the hologram matrix is

$$I_m = \frac{1}{N^2}\sum_{k=0}^{N-1}\sum_{l=0}^{N-1} I(k\Delta x, l\Delta y)$$
(3.27)

$r^2 + o^2$ now can be suppressed by subtracting this average intensity I_m from the hologram:

$$I'(k\Delta x, l\Delta y) = I(k\Delta x, l\Delta y) - I_m(k\Delta x, l\Delta y)$$
(3.28)

for $k = 0, \ldots, N - 1; l = 0, \ldots, N - 1$.

The reconstruction of I' results in an image free of the zero order.

Instead of subtracting the average intensity it is also possible to filter the hologram matrix by a high-pass with low cut-off frequency [44].

Another method for suppressing the DC term is to measure the intensities of the reference wave and object wave separately. However, this requires greater experimental effort due to the additional measurements required.

3.5. Spatial frequency limitation

The light-sensitive material used to record holograms must resolve the interference pattern resulting from superposition of the waves scattered from all object points and the reference wave. The maximum spatial frequency, which has to be resolved, is determined by the maximum angle θ_{max} between these waves [108]:

$$f_{max} = \frac{2}{\lambda}\sin\left(\frac{\theta_{max}}{2}\right).$$
(3.29)

Photographic emulsions used in optical holography have resolutions up to 5000 linepairs per millimetre (Lp mm^{-1}). With these materials, holograms with angles between the reference and the object wave of up to 180° can be recorded. However, the distance between neighbouring pixels of a CCD is only of the order of $\Delta x \approx 10~\mu$m. The corresponding maximum resolvable spatial frequency calculated by

$$f_{max} = \frac{1}{2\Delta x}$$
(3.30)

is therefore of the order of 50 Lp mm^{-1}. According to (3.29) the maximum angle between the reference and object wave is therefore limited to a few degrees. In this case the sine function in (3.29) can be approximated by the argument

$$f_{max} \approx \frac{\theta_{max}}{\lambda}.$$
(3.31)

3.6. Recording set-ups

Typical set-ups used in digital holography are shown in figure 11. In figure 11(a) a plane reference wave according to (3.3) is used, which propagates perpendicularly to the CCD. The object is located unsymmetrical with respect to the centre line. This set-up is very simple, but the space occupied by the object is not used effectively. In figure 11(b) the plane reference wave is coupled into the set-up via a beamsplitter. This allows us to position the object symmetrically. At a given
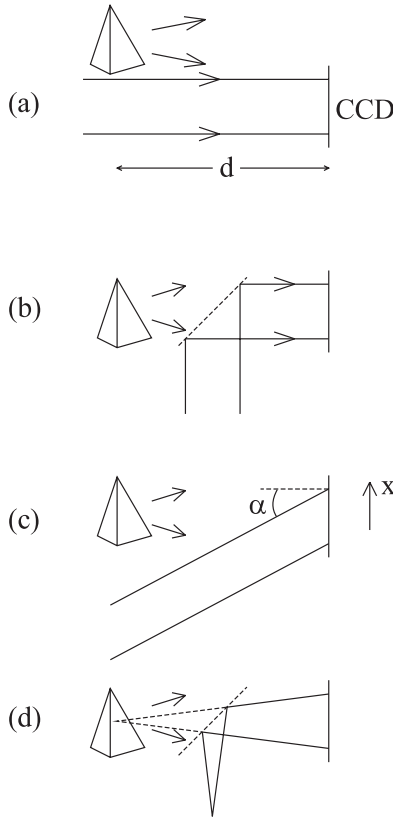
Figure 11. Recording set-ups.

distance d objects with larger dimensions can be recorded. However, the DC term is in the centre of the reconstructed image and has to be suppressed by the procedure described in section 3.4.

In figure 11(c) the reference wave impinges onto the CCD under an angle α. The reference wave is described by

$$R = \exp\left(-i\frac{2\pi}{\lambda}x\sin\alpha\right). \qquad (3.32)$$

Figure 11(d) is called *lensless Fourier holography*. It has been realized also in digital holography [39]. The point source of the spherical reference wave is located in the plane of the object:

$$R = \frac{\exp\left(-i\frac{2\pi}{\lambda}\sqrt{(d^2 + x^2 + y^2)}\right)}{\sqrt{(d^2 + x^2 + y^2)}}$$
$$\approx \frac{1}{d}\exp\left(-i\frac{2\pi}{\lambda}d\right)\exp\left(-i\frac{\pi}{\lambda d}(x^2 + y^2)\right). \qquad (3.33)$$

Again the Fresnel approximation is used for the square root. Inserting this expression into the reconstruction formula for the virtual image (3.10) leads to the following equation:

$$\Gamma(\xi, \eta) = C\exp\left[-i\frac{\pi}{\lambda d}(\xi^2 + \eta^2)\right]\Im^{-1}\{h(x, y)\} \qquad (3.34)$$

where C is a complex constant. A lensless Fourier hologram is therefore reconstructed by a Fourier transform. The effect of the spherical phase factor associated with the Fresnel transform is eliminated by the use of a spherical reference wave with the same curvature.

If objects with dimensions larger than a few centimetres are be recorded by CCDs, the recording distance d increases up to several metres. This is not feasible in practice. Therefore set-ups have been developed which reduce the object angle in order to make the spatial frequency spectrum resolvable [32, 109]. An example of such a set-up is shown in figure 12. A divergent lens is positioned between the object and the target. This lens generates a reduced virtual image of the object in a distance d'. The object wavefield is not recorded, but rather that of the reduced virtual image. The reference wave is superimposed by a beamsplitter.

3.7. Phase-shifting digital holography

The amplitude and phase of a light wave can be reconstructed from a single hologram by the methods described in the preceding sections. A completely different approach has been proposed by Skarman [56, 57]. He used a phase-shifting algorithm to calculate the *initial* phase and therefore the complex amplitude in a certain plane, e.g. the image plane or any other plane. With this initial complex amplitude it is possible to calculate the wave field in any other plane using the Fresnel–Kirchhoff integral. Later this phase-shifting digital holography was improved and applied to opaque objects by Yamaguchi *et al* [58–60, 62–64].

The principal arrangement for phase-shifting digital holography is shown in figure 13. The object wave and reference wave are interfering at the surface of a CCD. The reference wave is guided via a mirror mounted on a piezoelectric transducer (PZT). With this PZT the phase of the reference wave can be shifted stepwise. The principle of phase-shifting interferometry is to record several (at least three) interferograms with mutual phase shifts. The object phase φ_O is then calculated from these phase-shifted interferograms. We will not repeat here the various phase-shifting algorithms, but refer the reader to the literature, see, for example, [100]. The real amplitude $o(x, y)$ of the object wave can be measured from the intensity by blocking the reference wave.

As a result the complex amplitude

$$O(x, y) = o(x, y)\exp\left(+i\frac{2\pi}{\lambda}\varphi_O(x, y)\right) \qquad (3.35)$$

of the object wave is determined in the recording (x, y) plane.

Now we can use the Fresnel–Kirchhoff integral to calculate the complex amplitude in any other plane. An image of the object is calculated by introducing an artificial lens with $f = d/2$ according to (3.9) at the recording plane. With the Fresnel approximation the complex amplitude in the image plane is then calculated by

$$\Gamma(\xi, \eta) = C\exp\left[-i\frac{\pi}{\lambda d}(\xi^2 + \eta^2)\right]$$
$$\times \int_{-\infty}^{\infty}\int_{-\infty}^{\infty} O(x, y)L(x, y)\exp\left[-i\frac{\pi}{\lambda d}(x^2 + y^2)\right]$$
$$\times \exp\left[i\frac{2\pi}{\lambda d}(x\xi + y\eta)\right]dx\,dy$$
$$= C\exp\left[-\frac{i\pi}{\lambda d}(\xi^2 + \eta^2)\right]\int_{-\infty}^{\infty}\int_{-\infty}^{\infty} O(x, y)$$
$$\times \exp\left[+i\frac{\pi}{\lambda d}(x^2 + y^2)\right]\exp\left[i\frac{2\pi}{\lambda d}(x\xi + y\eta)\right]dx\,dy.$$
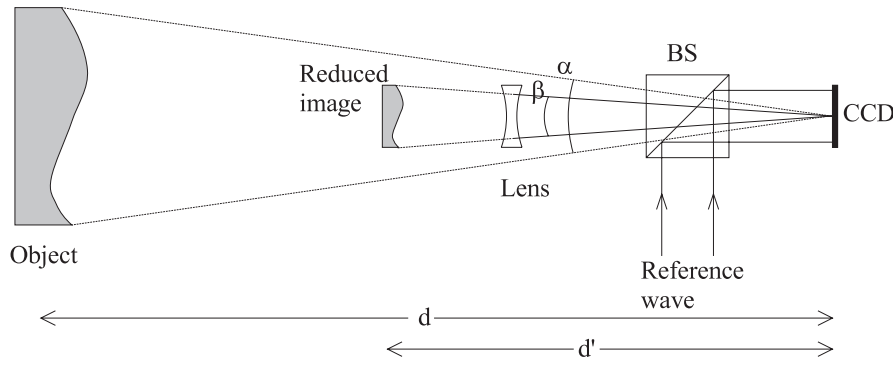$$(3.36)$$

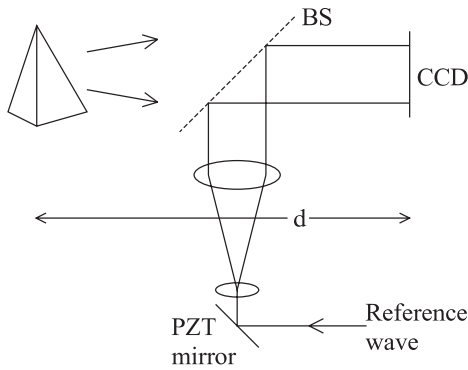**Figure 12.** Recording geometry for large objects.

Figure 13. Phase-shifting digital holography.

The advantage of phase-shifting digital holography is that the reconstructed image is free from the zero-order term and from the conjugate image. However, the price for this achievement is the higher technical effort: phase-shifted interferograms have to be generated, restricting the method to slowly varying phenomena with constant phase during the recording cycle.

4. Digital holographic interferometry

4.1. Deformation measurement

In conventional HI two waves, scattered from an object in different states, are superimposed. The resulting holographic interferogram carries information about the phase change between the waves in the form of dark and bright fringes. However, as described in section 2.2, the interference phase cannot be extracted unequivocally from a single interferogram. The interference phase is usually calculated from three or more phase-shifted interferograms by a phase-shifting algorithm. This requires additional experimental effort.

In digital holography a completely different way of processing is possible [19]. In each state of the object a digital hologram is recorded. Instead of superimposing these holograms as in conventional HI using photographic plates, the digital holograms are reconstructed separately according to the theory of section 3. From the resulting complex amplitudes $\Gamma_1(\xi, \eta)$ and $\Gamma_2(\xi, \eta)$ the phases are calculated:

$$\varphi_1(\xi, \eta) = \arctan \frac{\operatorname{Im} \Gamma_1(\xi, \eta)}{\operatorname{Re} \Gamma_1(\xi, \eta)} \qquad (4.1)$$

$$\varphi_2(\xi, \eta) = \arctan \frac{\operatorname{Im} \Gamma_2(\xi, \eta)}{\operatorname{Re} \Gamma_2(\xi, \eta)}. \qquad (4.2)$$

The index 1 denotes the first (undeformed) state and the index 2 is for the second (deformed) state. In (4.1) and (4.2) the phase takes values between $-\pi$ and π, the principal values of the arctan function. The interference phase is now calculated directly by subtraction:

$$\Delta\varphi = \begin{cases} \varphi_1 - \varphi_2 & \text{if } \varphi_1 \geqslant \varphi_2 \\ \varphi_1 - \varphi_2 + 2\pi & \text{if } \varphi_1 < \varphi_2. \end{cases} \qquad (4.3)$$

This equation permits the calculation of the interference phase directly from the digital holograms. The generation and evaluation of an interferogram is not necessary.

An example of digital HI is shown in figure 14. The upper left and upper right figures show two digital holograms, recorded at different states. Between the two recordings the knight has been tilted by a small amount. Each hologram is reconstructed separately by a numerical Fresnel transform. The reconstructed phases according to (4.1) and (4.2) are depicted in the two figures of the middle row. The phases vary randomly due to the surface roughness of the object. Subtraction of the phases according to (4.3) results in the interference phase, lower left figure.

The interference phase is indefinite to an additive multiple of 2π. The information about the additive constant is already lost in the holographic interferometric process. This is not a consequence of digital HI, but is valid for all interferometric methods using wavelength as a length unit. To convert the interference phase modulo 2π into a continual phase distribution, one can apply the standard phase unwrapping algorithm developed for conventional HI or ESPI. These phase unwrapping procedures are therefore not repeated here, instead we refer to textbooks (see, for example, [100, pp 161–70]). The unwrapped phase image of the example is shown in the lower right picture of figure 14. This plot corresponds to the object displacement, because the sensitivity vector is nearly constant and perpendicular over the whole surface.

An application of digital HI is the measurement of transient deformations due to impact loading [32, 109], because only one single recording is necessary in each deformation state. As an example, we present the transient deformation field of a plate made of fibre-reinforced material. The dimensions of the plate are 12 cm × 18 cm. Therefore the optical set-up of figure 14 is used for hologram recording

Figure 15. Interference phase modulo 2π.

3.5 µm

12 cm

18 cm

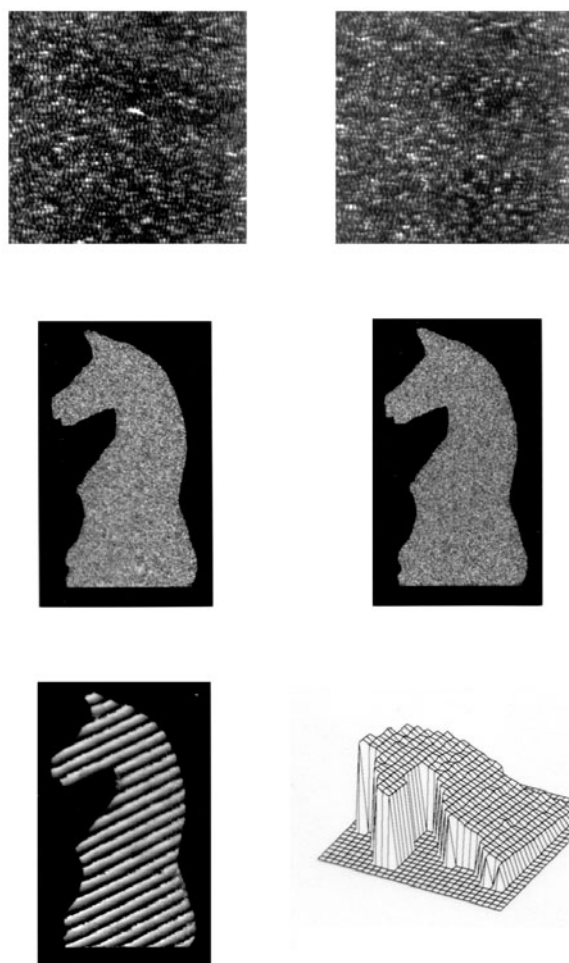**Figure 16.** Unwrapped phase, corresponding to deformation 5 µs after the impact.

Figure 14. Digital HI (from [110]).

in order to reduce the spatial frequencies. A pneumatically accelerated steel ball hits the plate and causes a transient deformation. Two holograms are recorded: the first exposure takes place before the impact, when the plate is at rest. The second hologram is recorded a few microseconds after the impact. The holograms are recorded by a pulsed ruby laser with a pulse duration of about 30 ns. The second hologram recording is triggered by a photoelectric barrier, which generates the start signal for the laser after the ball has crossed. As a typical result, the interference phase modulo 2π and the unwrapped phase are shown in figures 15 and 16. The unwrapped phase corresponds to the deformation field 5 µs after the impact.

4.2. Shape measurement

HI can produce an image of a three-dimensional object modulated by a fringe pattern corresponding to contours of constant elevation with respect to a reference plane [99, p 246]. The shape of the object is determined by these contour fringes and by the geometry of the recording set-up. Holographic contour fringes can be generated either by changing the recording wavelength (two-wavelength method), by varying the refractive index of the medium of light propagation (two-refractive index method) or by changing the angle of illumination.
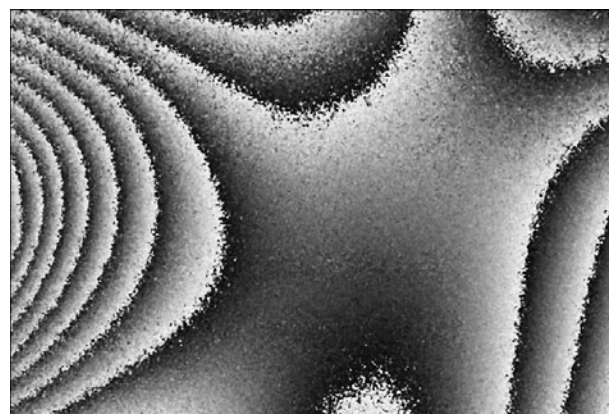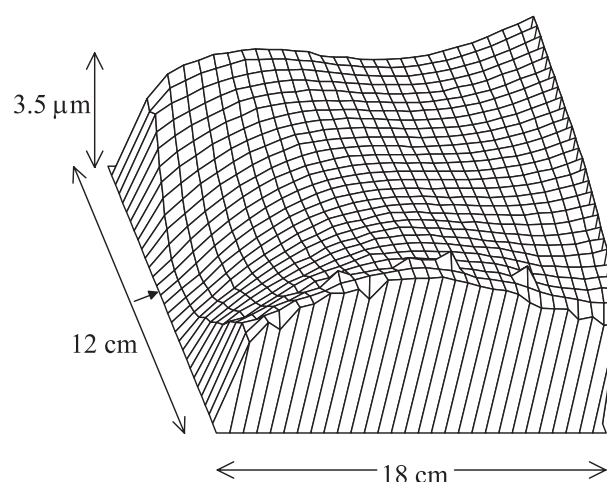
For shape measurement by the two-wavelength method two holograms are recorded with different wavelengths λ_1 and λ_2. In conventional HI both holograms are recorded on a single photographic plate. Both holograms are now reconstructed by one wavelength, e.g. λ_1. Therefore two images of the object are generated. The image recorded and reconstructed by λ_1 is an exact duplicate of the original object surface. The image which has been recorded with λ_1, but is reconstructed with λ_2, is slightly shifted in observation direction with respect to the original surface. These two reconstructed images interfere. For the special case of parallel illumination and observation directions which do not vary across the surface the following equation results for the height steps between neighbouring fringes:

$$\Delta H = \frac{\lambda_1 \lambda_2}{2|\lambda_1 - \lambda_2|} = \frac{\Lambda}{2}. \tag{4.4}$$

This equation is valid for small wavelength differences. The expression

$$\Lambda = \frac{\lambda_1 \lambda_2}{|\lambda_1 - \lambda_2|} \tag{4.5}$$

is called the *synthetic* or *equivalent* wavelength.

The concept of two-wavelength contouring has been introduced also into digital holography [20, pp 59–60], [39, 71]. Two holograms are recorded with λ_1 and λ_2 and

stored electronically. In contrast to conventional HI using photographic plates, both holograms can be reconstructed separately by the correct wavelengths, according to the theory of section 3. From the resulting complex amplitudes $\Gamma_{\lambda 1}(\xi, \eta)$ and $\Gamma_{\lambda 2}(\xi, \eta)$ the phases are calculated:

$$\varphi_{\lambda 1}(\xi, \eta) = \arctan \frac{\operatorname{Im} \Gamma_{\lambda 1}(\xi, \eta)}{\operatorname{Re} \Gamma_{\lambda 1}(\xi, \eta)} \qquad (4.6)$$

$$\varphi_{\lambda 2}(\xi, \eta) = \arctan \frac{\operatorname{Im} \Gamma_{\lambda 2}(\xi, \eta)}{\operatorname{Re} \Gamma_{\lambda 2}(\xi, \eta)}. \qquad (4.7)$$

As for deformation analysis the phase difference is now calculated directly by subtraction:

$$\Delta\varphi = \begin{cases} \varphi_{\lambda 1} - \varphi_{\lambda 2} & \text{if } \varphi_{\lambda 1} \geqslant \varphi_{\lambda 2} \\ \varphi_{\lambda 1} - \varphi_{\lambda 2} + 2\pi & \text{if } \varphi_{\lambda 1} < \varphi_{\lambda 2}. \end{cases} \qquad (4.8)$$

This phase map is equivalent to the phase distribution of a hologram recorded with the synthetic wavelength Λ. A 2π phase jump corresponds to a height step of $\Lambda/2$.

One advantage of digital holography contouring is that both holograms are reconstructed with the correct wavelength. Distortions resulting from hologram reconstruction with a different wavelength than the recording wavelength, as in optical contouring, are therefore avoided. The other advantage is that the phase map according to (4.8) is calculated directly from the holograms, without generating an interference pattern. Recently digital holographic contouring with a wavelength difference of $\Delta\lambda = 25$ nm, corresponding to a synthetic wavelength of $\Lambda = 10$ μm and a depth resolution of 0.5 μm (1/20 period), has been demonstrated [112].

A modified contouring approach, which is referred to as multiwavelength or wavelength scanning contouring, is to use more than two illumination wavelengths to eliminate ambiguities inherent to modulo 2π phase distributions [53, 86, 90, 111]. The advantage of this technique is that it can also be used with objects that have phase steps or isolated object areas.

4.3. Measurement of refractive index variations

Another application of digital HI is the measurement of refractive index variations within transparent media [72, 74]. Effects that influence the refractive index can be investigated by this method. These effects are, for example, temperature gradients in fluids or concentration variations in crystal growth experiments.

A refractive index change in a transparent medium leads to a change of the optical path length and thereby to an interference phase between two light waves passing the medium before and after the change. The interference phase due to refractive index variations is given by [99, p 217]

$$\Delta\varphi(x, y) = \frac{2\pi}{\lambda} \int_{l_1}^{l_2} [n(x, y, z) - n_0] \, \mathrm{d}z \qquad (4.9)$$

where n_0 is the refractive index of the medium under observation in its initial, unperturbed state and $n(x, y, z)$ is the final refractive index distribution. The light passes the medium in the z direction and the integration is taken along the propagation direction. Equation (4.9) is valid for small
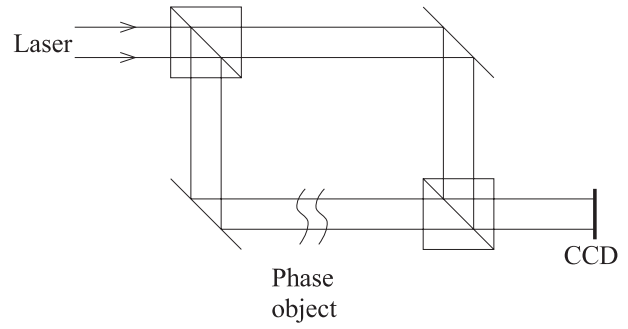

Figure 17. Recording set-up for transparent phase objects.

refractive index gradients, where the light rays propagate along straight lines. The simplest case is that of a two-dimensional phase object with no variation of refractive index in the z direction. In this case the refractive index distribution $n(x, y)$ can be calculated directly from (4.9). In the general case of a refractive index varying also in the z direction (4.9) cannot be solved without further information about the process. However, in many practical experiments only two-dimensional phase objects have to be considered.

Figure 17 shows a set-up used in digital HI. The expanded laser beam is divided into reference and object beams. The object passes the transparent phase object and illuminates the CCD. The reference beam impinges directly on the CCD. Both beams interfere and the hologram is digitally recorded. The set-up is very similar to a conventional Mach–Zehnder interferometer. The difference is that the interference figure is here interpreted as a hologram, which can be reconstructed with the theory of section 3. Therefore all features of digital holography, like direct access to the phase or numerical refocusing, are available.

As for deformation analysis two digital holograms are recorded. The first exposure takes place before, and the second after, the refractive index change. These digital holograms are reconstructed numerically. From the resulting complex amplitudes $\Gamma_1(\xi, \eta)$ and $\Gamma_2(\xi, \eta)$ the phases are calculated by (4.1) and (4.2). Finally the interference phase is calculated by subtracting according to (4.3).

In the reconstruction of holograms recorded by the set-up of figure 17 the undiffracted reference wave, the real image and the virtual image are superimposed. This overlapping disturbs the image. The undiffracted reference wave can be suppressed by filtering with the methods discussed in section 3.4. The overlapping of the unwanted twin image (either the virtual image, if one focuses on the real image, or vice versa) can be avoided by slightly tilting one of the interfering waves. In this case the images are spatially separated.

The interferometer of figure 17 is sensitive to local disturbances due to imperfections in optical components or dust particles. The influence of these disturbances can be minimized if a diffusing screen is placed in front of or behind the phase object. In this case the unfocused twin image appears only as a diffuse background in the images, which does not disturb the evaluation. In addition, if a diffuser is introduced, tilting of the interfering waves is not necessary for image separation. A disadvantage of using a diffuser is the generation of speckles due to the rough surface.
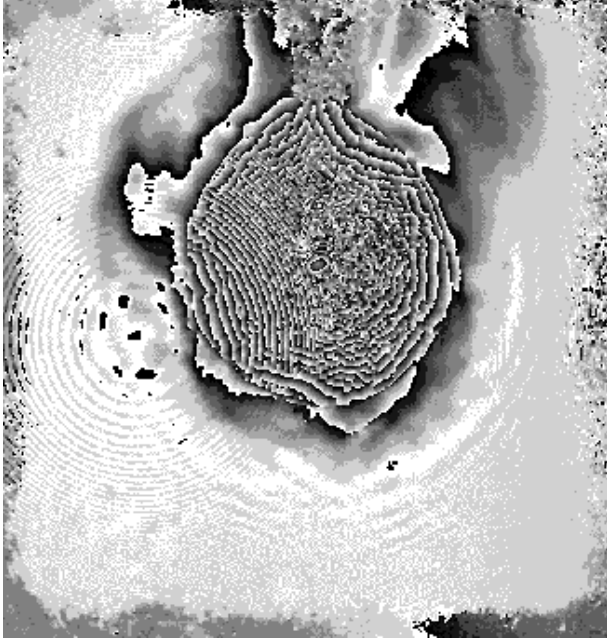
Figure 18. Interference phase modulo 2π of a liquid system (from [74]).
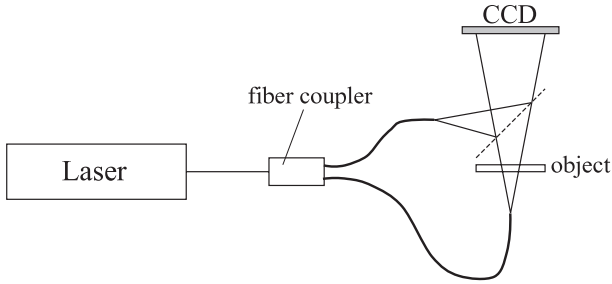

Figure 19. Digital holographic microscope.

In figure 18 a typical interference modulo 2π image of a transparent phase object is shown. The holograms are recorded with the set-up of figure 17 (without diffuser). The object volume consists of a droplet of toluene, which is introduced into the water/acetone liquid phase. The refractive index changes are caused by a concentration gradient, which is induced by the mass transfer of acetone into the droplet.

5. Digital holographic microscopy

Another application of digital holography is microscopy, where the depth of focus is very limited due to the high magnification. The investigation of a three-dimensional object with microscopic resolution requires certain refocusing steps. Digital holography offers the possibility to focus on different object layers by numerical methods. In addition, the images are free of aberrations due to the imperfections of optical lenses. Fundamental work in the field of digital holographic microscopy has been done by Haddad *et al* [73].

In order to obtain a high lateral resolution $\Delta\xi$ in the reconstructed image the object has to be placed near to the CCD. The necessary distance can be estimated by (3.16). With a pixel size of $\Delta x = 10\ \mu$m, a wavelength of $\lambda = 500$ nm,

1000 $\times$ 1000 pixels and a required resolution of $\Delta\xi = 1\ \mu$m a distance of $d = 2$ cm results[4]. However, at such short distances the Fresnel approximation is no longer valid. The convolution approach has to be applied. On the other hand, the resolution of an image calculated by this approach is determined by the pixel size of the CCD, see (3.25). Typical pixel sizes for high resolution cameras are in the range of 10 μm $\times$ 10 μm, too low for microscopy. Therefore the reconstruction procedure has to be modified [104].

The lateral magnification of the holographic reconstruction can be derived from the holographic imaging equations. The lateral magnification of the reconstructed virtual image is [99, p 25]

$$M = \left[1 + \frac{d}{d'_r}\frac{\lambda_1}{\lambda_2} - \frac{d}{d_r}\right]^{-1} \quad (5.1)$$

where d_r and d'_r describe the distances between the source point of a spherical reference wave and the hologram plane in the recording and reconstruction process, respectively. λ_1 and λ_2 are the wavelengths for recording and reconstruction. The reconstruction distance d', i.e. the position of the reconstructed image, can be calculated by

$$d' = \left[\frac{1}{d'_r} + \frac{\lambda_2}{\lambda_1}\frac{1}{d} - \frac{1}{d_r}\frac{\lambda_2}{\lambda_1}\right]^{-1}. \quad (5.2)$$

If the same reference wavefront is used for recording and reconstruction it follows that $d' = d$. Note that d, d', dr and dr' are always counted positive in this work.

Magnification can be introduced by changing the wavelength or position of the source point of the reference wave in the reconstruction process. In digital holography the magnification can be easily introduced by changing d'_r. If the desired magnification factor is determined the reconstruction distance can be calculated using (5.1) and (5.2) with $\lambda_1 = \lambda_2$:

$$d' = dM. \quad (5.3)$$

The magnification can be introduced by placing the source point of the reference wave at a distance

$$d'_r = \left[\frac{1}{d'} - \frac{1}{d} + \frac{1}{d_r}\right]^{-1}. \quad (5.4)$$

The reference wave is now described by

$$R(x,y) = \exp\left(-i\frac{2\pi}{\lambda}\sqrt{d'^2_r + (x-x'_r)^2 + (y-y'_r)^2}\right) \quad (5.5)$$

where $(x'_r, y'_r, -d'_r)$ is the position of the reference source point in the reconstruction process.

A set-up for digital holographic microscopy is shown in figure 19. The object is illuminated in transmission and the spherical reference wave is coupled to the set-up via a semi-transparent mirror. Reference and object waves are guided via optical fibres. A digital hologram of a USAF target recorded with this set-up is shown in figure 20. The corresponding intensity reconstruction is depicted in figure 21. The resolution is about 2.2 μm. We want to emphasize that, due to the change of the reference source point in the reconstruction process, aberrations are introduced, which limit the achievable resolution.

---

[4] This is only an estimate, since equation (3.16) is not valid at short distances.
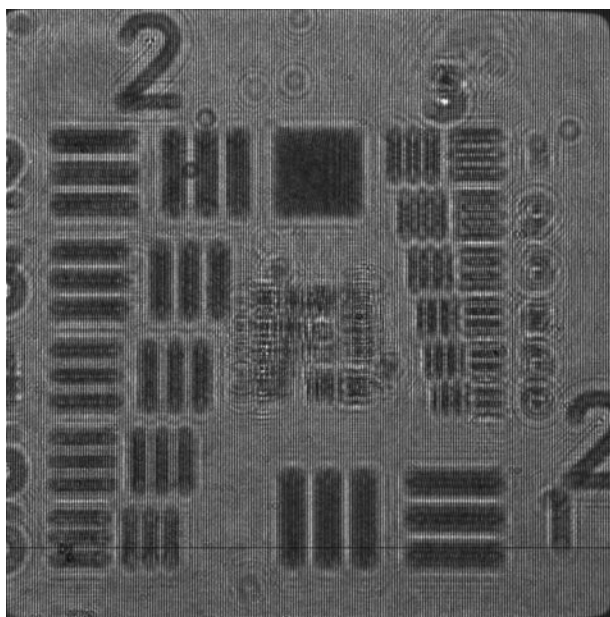
Figure 20. Digital hologram (from [104]).

Figure 21. Numerical reconstruction with microscopic resolution.

Phase-shifting digital holography has also been applied to microscopy [59, 60, 63]. In this case an ordinary microscope is used for image generation. The reference wave is superimposed in the image plane. After generation of the initial phase by phase-shifting, as described in section 3.7, one can focus on other planes by numerical methods. The quality of the refocused images can be improved if a source of partial spatial coherence is used for hologram recording [61].

6. Concluding remarks

Digital holography has been established as an important scientific tool for applications in imaging, microscopy, interferometry and other optical disciplines. The method is characterized by the following features:

- No wet-chemical or other processing of holograms.
- From one digital hologram different object planes can be reconstructed by numerical methods (numerical focusing).
- Lensless imaging, i.e. no aberrations by imaging devices.
- Direct phase reconstruction, i.e. phase differences in HI can be calculated directly from holograms, without interferogram generation and processing.

Digital HI is a competing technique to electronic speckle pattern interferometry. ESPI has been used for many years in real time, i.e. the recording speed is only limited by the frame rate of the recording device (CCD). In contrast to ESPI, digital holography needs time for running the reconstruction algorithm. However, the reconstruction time has been reduced drastically in recent years due to the progress in computer technology. Digital holograms with 1000×1000 pixels can nowadays be reconstructed almost in real time. It may be expected therefore that the acceptance of digital holography will increase in the future.
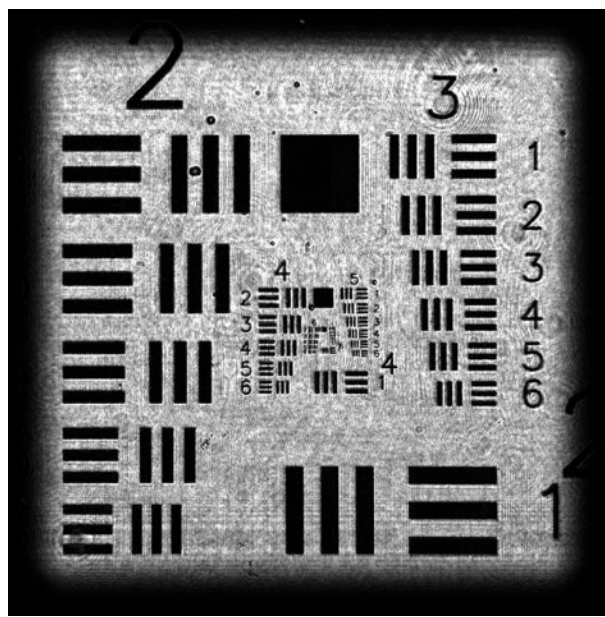
References

[1] Gabor D 1948 A new microscopic principle *Nature* **161** 777–8
[2] Gabor D 1949 Microscopy by reconstructed wavefronts *Proc. R. Soc.* **197** 454–87
[3] Gabor D 1951 Microscopy by reconstructed wavefronts: *Proc. Phys. Soc.* **64** 449–69
[4] Leith E N and Upatnieks J 1962 Reconstructed wavefronts and communication theory *J. Opt. Soc. Am.* **52** 1123–30
[5] Leith E N and Upatnieks J 1964 Wavefront reconstruction with diffused illumination and three-dimensional objects *J. Opt. Soc. Am.* **54** 1295–301
[6] Powell R L and Stetson K A 1965 Interferometric vibration analysis by wavefront reconstructions *J. Opt. Soc. Am.* **55** 1593–8
[7] Stetson K A and Powell R L 1965 Interferometric hologram evaluation and real-time vibration analysis of diffuse objects *J. Opt. Soc. Am.* **55** 1694–5
[8] Lee W H 1978 Computer-generated holograms: techniques and applications *Prog. Opt.* **16** 120–232
[9] Bryngdahl O and Wyrowski F 1990 Digital holography—computer generated holograms *Prog. Opt.* **28** 1–86
[10] Schreier D 1984 *Synthetische Holografie* (Weinheim: VCH)
[11] Kronrod M A, Yaroslavski L P and Merzlyakov N S 1972 Computer synthesis of transparency holograms *Sov. Phys.–Tech. Phys.* **17** 329–32
[12] Kronrod M A, Merzlyakov N S and Yaroslavski L P 1972 Reconstruction of holograms with a computer *Sov. Phys.–Tech. Phys.* **17** 333–4
[13] Yaroslavskii L P and Merzlyakov N S 1980 *Methods of Digital Holography* (New York: Consultants Bureau)
[14] Onural L and Scott P D 1987 Digital decoding of in-line holograms *Opt. Eng.* **26** 1124–32
[15] Liu G and Scott P D 1987 Phase retrieval and twin-image elimination for in-line Fresnel holograms *J. Opt. Soc. Am.* A **4** 159–65
[16] Onural L and Özgen M T 1992 Extraction of three-dimensional object-location information directly from in-line holograms using Wigner analysis *J. Opt. Soc. Am.* A **9** 252–60
[17] Schnars U and Jüptner W 1993 Principles of direct holography for interferometry *FRINGE 93: Proc. 2nd Int.*

Workshop on Automatic Processing of Fringe Patterns ed W Jüptner and W Osten (Berlin: Akademie) pp 115–20

[18] Schnars U and Jüptner W 1994 Direct recording of holograms by a CCD-target and numerical reconstruction *Appl. Opt.* **33** 179–81

[19] Schnars U 1994 Direct phase determination in hologram interferometry with use of digitally recorded holograms *J. Opt. Soc. Am.* A **11** 2011–5 (Reprinted in: Hinsch K and Sirohi R (ed) 1997 *Holographic Interferometry—Principles and Techniques (SPIE Milestone Series vol 144)* pp 661–5)

[20] Schnars U 1994 Digitale aufzeichnung und mathematische rekonstruktion von hologrammen in der interferometrie *VDI-Fortschritt-Berichte (series 8 no 378)* (Düsseldorf: VDI)

[21] Schnars U and Jüptner W 1994 Digital reconstruction of holograms in hologram interferometry and shearography *Appl. Opt.* **33** 4373–7 (Reprinted in, Hinsch K and Sirohi R (ed) 1997 *Holographic Interferometry—Principles and Techniques (SPIE Milestone Series vol 144)* pp 656–60)

[22] Butters J N and Leendertz J A 1971 Holographic and videotechniques applied to engineering measurements *J. Meas. Control* **4** 349–54

[23] Macovski A, Ramsey D and Schaefer L F 1971 Time lapse interferometry and contouring using television systems *Appl. Opt.* **10** 2722–7

[24] Schwomma O 1972 *Austrian Patent* 298, 830

[25] Lokberg O 1980 Electronic speckle pattern interferometry *Phys. Technol.* **11** 16–22

[26] Stetson K A and Brohinsky R 1985 Electrooptic holography and its application to hologram interferometry *Appl. Opt* **24** 3631–7

[27] Creath K 1985 Phase shifting speckle-interferometry *Appl. Opt.* **24** 3053–8

[28] Stetson K A and Brohinsky R 1987 Electrooptic holography system for vibration analysis and nondestructive testing *Opt. Eng.* **26** 1234–9

[29] Lokberg O and Slettemoen G A 1987 Basic electronic speckle pattern interferometry *Appl. Opt. Opt. Eng.* **10** 455–505

[30] Doval A F 2000 A systematic approach to TV holography *Meas. Sci. Technol.* **11** R1–36

[31] Schnars U and Jüptner W 1994 Digitale Holografie—ein neues Verfahren der Lasermeßtechnik *Laser Optoelektron.* **26** 40–5

[32] Schnars U, Kreis T and Jüptner W 1996 Digital recording and numerical reconstruction of holograms: reduction of the spatial frequency spectrum *Opt. Eng.* **35** 977–82

[33] Schnars U, Geldmacher J, Hartmann H J and Jüptner W 1995 Mit digitaler Holografie den Stoßwellen auf der Spur *F&M* **103** 338–41

[34] Schnars U, Kreis T and Jüptner W 1995 CCD recording and numerical reconstruction of holograms and holographic interferograms *Proc. SPIE* **2544** 57–63

[35] Schnars U, Kreis T and Jüptner W 1995 Numerische rekonstruktion von hologrammen in der interferometrischen Meßtechnik *Proc. LASER 95* ed W Waidelich (Berlin: Springer)

[36] Pedrini G, Fröning P, Fessler H and Tiziani H J 1998 In-line digital holographic interferometry *Appl. Opt.* **37** 6262–9

[37] Cuche E, Bevilacqua F and Depeursinge C 1999 Digital holography for quantitative phase-contrast imaging *Opt. Lett.* **24** 291–3

[38] Pedrini G, Schedin S and Tiziani H 1999 Lensless digital holographic interferometry for the measurement of large objects *Opt. Commun.* **171** 29–36

[39] Wagner C, Seebacher S, Osten W and Jüptner W 1999 Digital recording and numerical reconstruction of lensless Fourier holograms in optical metrology *Appl. Opt.* **38** 4812–20

[40] Cuche E, Marquet P and Depeusinge C 2000 Spatial filtering for zero-order and twin-image elimination in digital off-axis holography *Appl. Opt.* **39** 4070–5

[41] Papp Z and Janos K 2001 Digital holography by two reference beams *Proc. SPIE* **4416** 112–15

[42] Xu L, Miao J and Asundi A 2000 Properties of digital holography based on in-line configuration *Opt. Eng.* **39** 3214–9

[43] Kreis T and Jüptner W 1997 Principles of digital holography *Proc. 3rd Int. Workshop on Automatic Processing of Fringe Patterns* ed W Jüptner and W Osten (Berlin: Akademie) pp 353–63

[44] Kreis T and Jüptner W 1997 Suppression of the dc term in digital holography *Opt. Eng.* **36** 2357–60

[45] Kreis T, Jüptner W and Geldmacher J 1998 Digital holography: methods and applications *Proc. SPIE* **3407** 169–77

[46] Kreis T, Jüptner W and Geldmacher J 1998 Principles of digital holographic interferometry *Proc. SPIE* **3478** 45–54

[47] Kim S, Lee B and Kim E 1997 Removal of bias and the conjugate image in incoherent on-axis triangular holography and real-time reconstruction of the complexhologram *Appl. Opt.* **36** 4784–91

[48] Lai S, Kemper B and von Bally G 1999 Off-axis reconstruction of in-line holograms for twin-image elimination *Opt. Commun.* **169** 37–43

[49] Yang S, Xie X, Thuo Y and Jia C 1999 Reconstruction of near-field in-line holograms *Opt. Commun.* **159** 29–31

[50] Grilli S, Ferraro P, De Nicola S, Finizio A, Pierattini G and Meucci R 2001 Whole optical wavefield reconstruction by digital holography *Opt. Express* **9** 294–302

[51] Schnars U, Hartmann H J and Jüptner W 1995 Digital recording and numerical reconstruction of holograms for nondestructive testing *Proc. SPIE* **2545** 250–3

[52] Kolenovic E, Lai S, Osten W and Jüptner W 2001 Endoscopic shape and deformation measurement by means of digital holography *Proc. 4th Int. Workshop on Automatic Processing of Fringe Patterns* ed W Jüptner and W Osten (Berlin: Akademie) pp 686–91

[53] Osten W, Seebacher S, Baumbach T and Jüptner W 2001 Absolute shape control of microcomponents using digital holography and multiwavelength contouring *Proc. SPIE* **4275** 71–84

[54] Osten W, Seebacher S and Jüptner W 2001 Application of digital holography for the inspection of microcomponents *Proc. SPIE* **4400** 1–15

[55] Seebacher S 2001 *Anwendung der Digitalen Holografie bei der 3D-Form-und Verformungsmessung an Komponenten der Mikrosystemtechnik* (Bremen: University of Bremen Publishing House)

[56] Wozniak K and Skarman B 1994 Digital holography in flow visualization *Final Report for ESA/ESTEC* (purchase order 142722)

[57] Skarman B, Becker J and Wozniak K 1996 Simultaneous 3D-PIV and temperature measurements using a new CCD-based holographic interferometer *Flow Meas. Instrum.* **7** 1–6

[58] Yamaguchi I and Zhang T 1997 Phase-shifting digital holography *Opt. Lett.* **22** 1268–70

[59] Zhang T and Yamaguchi I 1998 Three-dimensional microscopy with phase-shifting digital holography *Opt. Lett.* **23** 1221–3

[60] Yamaguchi I, Kato J, Ohta S and Mizuno J 2001 Image formation in phase-shifting digital holography and applications to microscopy *Appl. Opt.* **40** 6177–86

[61] Dubois F, Joannes L and Legros J C 1999 Improved three-dimensional imaging with a digital holography microscope with a source of partial spatial coherence *Appl. Opt.* **38** 7085–94

[62] Yamaguchi I, Inomoto O and Kato J 2001 Surface shape measurement by phase shifting digital holography *Proc. 4th Int. Workshop on Automatic Processing of Fringe Patterns* ed W Jüptner and W Osten (Berlin: Akademie) pp 365–72

[63] Zhang T and Yamaguchi I 1998 3D microscopy with phase-shifting digital holography *Proc. SPIE* **3479** 152–9

[64] Inomoto O and Yamaguchi I 2001 Measurements of Benard–Marangoni waves using phase-shifting digital holography *Proc. SPIE* **4416** 124–7

[65] Schnars U, Osten W, Jüptner W and Sommer K 1995 Advances of digital holography for experiment diagnostics in space *Proc. 46th Int. Astronautical Congress Oslo* Paper no IAF-95-J.5.01

[66] Adams M, Kreis T and Jüptner W 1999 Particle measurement with digital holography *Proc. SPIE* **3823**

[67] Adams M, Kreis T and Jüptner W 1997 Particle size and position measurement with digital holography *Proc. SPIE* **3098** 234–40

[68] Kreis T, Adams M and Jüptner W 1999 Digital in-line holography in particle measurement *Proc. SPIE* **3744**

[69] Owen R B and Zozulya A A 2000 In-line digital holographic sensor for monitoring and characterizing marine particulates *Opt. Eng.* **39** 2187–97

[70] Xu L, Peng X, Miao J and Asundi A K 2001 Studies of digital microscopic holography with applications to microstructure testing *Appl. Opt.* **40** 5046–51

[71] Seebacher S, Osten W and Jüptner W 1998 Measuring shape and deformation of small objects using digital holography *Proc. SPIE* **3479** 104–15

[72] Kebbel V, Grubert B, Hartmann H J, Jüptner W and Schnars U 1998 Application of digital holography to space-borne fluid science measurements *Proc. 49th Int. Astronautical Cong. (Melbourne)* (Paris: IAF) Paper no IAF-98-J.5.03

[73] Haddad W, Cullen D, Solem J C, Longworth J M, McPherson A, Boyer K and Rhodes C K 1992 Fourier-transform holographic microscope *Appl. Opt.* **31** 4973–8

[74] Kebbel V, Adams M, Hartmann H J and Jüptner W 1999 Digital holography as a versatile optical diagnostic method for microgravity experiments *Meas. Sci. Technol.* **10** 893–9

[75] Dubois F, Joannes L, Dupont O, Dewandel J L and Logros J C 1999 An integrated optical set-up for fluid-physics experiments under microgravity conditions *Meas. Sci. Technol.* **10** 934–45

[76] Javidi B and Nomura T 2000 Securing information by use of digital holography *Opt. Lett.* **25** 28–30

[77] Tajahuerce E and Javidi B 2000 Encrypting three-dimensional information with digital holography *Appl. Opt.* **39** 6595–601

[78] Pomarico J, Schnars U, Hartmann H J and Jüptner W 1996 Digital recording and numerical reconstruction of holograms: a new method for displaying light-in-flight *Appl. Opt.* **34** 8095–9

[79] Jüptner W, Pomarico J and Schnars U 1996 Light-in-flight measurements by digital holography *Proc. SPIE* **2860**

[80] Nilsson B and Carlsson T 1998 Direct three-dimensional shape measurement by digital light-in-flight holography *Appl. Opt.* **37** 7954–9

[81] Nilsson B and Carlsson T 1999 Digital light-in-flight holography for simultaneous shape and deformation measurement *Proc. SPIE* **3835** 127–34

[82] Nilsson B and Carlsson T 2000 Simultaneous measurement of shape and deformation using digital light-in-flight recording by holography *Opt. Eng.* **39** 244–53

[83] Carlsson T, Nilsson B and Gustafsson J 2001 System for acquisition of three-dimensional shape and movement using digital light-in-flight holography *Opt. Eng.* **40** 67–75

[84] Osten W, Baumbach T, Seebacher S and Jüptner W 2001 Remote shape control by comparative digital holography *Proc. 4th Int. Workshop on Automatic Processing of Fringe Patterns* ed W Jüptner and W Osten (Berlin: Akademie) pp 373–82

[85] Lai S, King B and Neifeld M A 2000 Wave front reconstruction by means of phase-shifting digital in-line holography *Opt. Commun.* **173** 155–60

[86] Kim M K 2000 Tomographic three-dimensional imaging of a biological specimen using wavelength-scanning digital interference holography *Opt. Express* **7** 305–10

[87] Frauel Y and Javidi B 2001 Neural network for three-dimensional object recognition based on digital holography *Opt. Lett.* **26** 1478–80

[88] De Nicola S, Ferraro P, Finizio A and Pierattini G 2001 *Opt. Lett.* **26** 974–6

[89] Stadelmaier A and Massig J H 2000 Compensation of lens aberrations in digital holography *Opt. Lett.* **25** 1630–2

[90] Kim M K 1999 Wavelength-scanning digital interference holography for optical section imaging *Opt. Lett.* **24** 1693–5

[91] Le Clerc F, Collot L and Gross M 2000 Numerical heterodyne holography with two-dimensional photodetector arrays *Opt. Lett.* **25** 716–18

[92] Javidi B and Tajahuerce E 2000 Three-dimensional object recognition by use of digital holography *Opt. Lett.* **25** 610–12

[93] Takaki Y, Kawai H and Ohzu H 1999 Hybrid holographic microscopy free of conjugate and zero-order images *Appl. Opt.* **38** 4990–6

[94] Tajahuerce E, Matoba O and Javidi B 2001 Shift-invariant three-dimensional object recognition by means of digital holography *Appl. Opt.* **40** 3877–86

[95] Onural L 2000 Sampling of the diffraction field *Appl. Opt.* **39** 5929–35

[96] Grunwald R, Griebner U, Elsaesser T, Kebbel V, Hartmann H J and Jüptner W 2001 Femtosecond interference experiments with thin-film micro-optical components *Proc. 4th Int. Workshop on Automatic Processing of Fringe Patterns* ed W Jüptner and W Osten (Berlin: Akademie) pp 33–40

[97] De Nicola S, Ferraro P, Finizio A and Pierattini G 2001 Compensation of Aberrations in Fresnel off-axis Digital Holography *Proc. 4th Int. Workshop on Automatic Processing of Fringe Patterns* ed W Jüptner and W Osten (Berlin: Akademie) pp 407–12

[98] Kreis T, Aswendt P and Höfling R 2001 Hologram reconstruction using a digital micromirror device *Opt. Eng.* **40** 926–33

[99] Harriharan P 1984 *Optical Holography* (Cambridge: Cambridge University Press)

[100] Kreis T 1996 *Holographic Interferometry* (Berlin: Akademie)

[101] Jüptner W 1978 Automatisierte auswertung holografischer interferogramme mit dem Zeilen–Scanverfahren *Proc. Frühjahrsschule 78 Holografische Interferometrie in Technik und Medizin (DGaO)* ed H H Kreitlow and W Jüptner

[102] Jüptner W, Kreis T and Kreitlow H 1983 Automatic evaluation of holographic interferograms by reference beam phase shifting *Proc. SPIE* **398** 22–9

[103] Sollid J E 1969 Holographic interferometry applied to measurements of small static displacements of diffuselyreflecting surfaces *Appl. Opt.* **8** 1587–95

[104] Kebbel V, Hartmann H-J and Jüptner W 2001 Application of digital holographic microscopy for inspection of micro-opticalcomponents *Proc. SPIE* **4398** 189–98

[105] Klein M V and Furtak T E 1988 *Optik* German edn (Berlin: Springer)

[106] Brigham E O 1974 *The Fast Fourier Transform* (Englewood Cliffs, NJ: Prentice-Hall)

[107] Demetrakopoulos T H and Mittra R 1974 Digital and optical reconstruction of images from suboptical diffraction patterns *Appl. Opt* **13** 665–70

[108] Ostrovsky Y I, Butosov M M and Ostrovskaja G V 1980 *Interferometry by Holography* (New York: Springer)

[109] Pedrini G, Zou Y L and Tiziani H 1995 Digital double-pulsed holographic interferometry for vibration analysis *J. Mod. Opt.* **42** 367–74

[110] Schnars U and Jüptner W 1995 Digitale Holografie (Handout) *Annual Conf. of the Deutsche Gesellschaft für Angewandte Optik*

[111] Wagner C, Osten W and Seebacher S 2000 Direct shape measurement by digital wavefront reconstruction andmultiwavelength contouring *Opt. Eng.* **39** 79–85

[112] Jüptner W 2000 Qualität durch Lasertechnik–Zukunft für das 21. Jahrhundert *Proc. LEF Symp. (Erlangen)*